Engineering the Structure and Properties of DNA-Nanoparticle Superstructures Using Polyvalent Counterions

Leo Y. T. Chou,[†,∇,#] Fayi Song,[†,∇] and Warren C. W. Chan*[†,‡,§,∥,⊥]

[†]Institute of Biomaterials and Biomedical Engineering, Rosebrugh Building, Room 407, 164 College Street, Toronto, Ontario M5S 3G9, Canada

[‡]Terrence Donnelly Centre for Cellular and Biomolecular Research, University of Toronto, 160 College Street, Room 230, Toronto, Ontario M5S 3E1, Canada

[§]Department of Chemical Engineering, University of Toronto, 200 College Street, Toronto, Ontario M5S 3E5, Canada

[∥]Department of Chemistry, University of Toronto, 80 St George Street, Toronto, Ontario M5S 3H6, Canada

[⊥]Department of Material Science and Engineering, University of Toronto, Wallberg Building, 184 College Street, Suite 140, Toronto, Ontario M5S 3E4, Canada

S *Supporting Information*

ABSTRACT: DNA assembly of nanoparticles is a powerful approach to control their properties and prototype new materials. However, the structure and properties of DNA-assembled nanoparticles are labile and sensitive to interactions with counterions, which vary with processing and application environment. Here we show that substituting polyamines in place of elemental counterions significantly enhanced the structural rigidity and plasmonic properties of DNA-assembled metal nanoparticles. These effects arose from the ability of polyamines to condense DNA and cross-link DNA-coated nanoparticles. We further used polyamine wrapped DNA nanostructures as structural templates to seed the growth of polymer multilayers via layer-by-layer assembly, and controlled the degree of DNA condensation, plasmon coupling efficiency, and material responsiveness to environmental stimuli by varying polyelectrolyte composition. These results highlight counterion engineering as a versatile strategy to tailor the properties of DNA-nanoparticle assemblies for various applications, and should be applicable to other classes of DNA nanostructures.
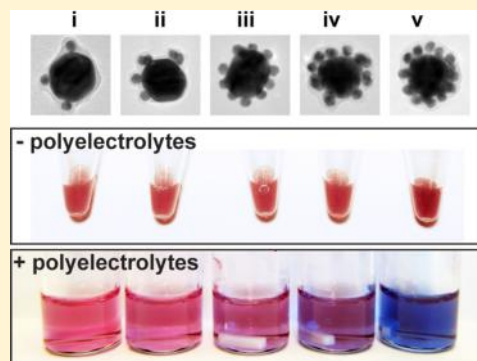
INTRODUCTION

Molecular assembly using DNA benefits from its well-defined structure, sequence programmability, and robust Watson–Crick pairing rules.[1] These advantages have been exploited in the field of nanotechnology to control nanoparticle properties by assembling them into supramolecular materials.[2,3] The structure and properties of such materials are known to be sensitive to DNA interactions with counterions such as sodium or magnesium. Cations are commonly used to facilitate DNA hybridization by screening electrostatic repulsion between the DNA phosphate backbone, and are especially important for nanoparticle assemblies in which DNA strands are densely packed.[4,5] Charge screening using counterions has been shown to enhance the properties of nanoparticle assemblies that derive from nanoparticle coupling,[6] and in some cases give rise to novel properties of nanoparticle assemblies such as cooperative melting[5,7] and resistance to nucleases.[8] On the other hand, counterion sensitivity also limits downstream applications of DNA-assembled nanoparticles. First, it renders them structurally labile[9,10] and incompatible with some solid-state fabrication processes. Second, while high ionic strength solvents have previously been used to enhance the properties of DNA-

assembled nanoparticles such as plasmon coupling,[3,6,11] high salts can also induce nanoparticle aggregation, making this strategy unsuitable for solution-based applications. Finally, for biological uses such as intracellular sensing and drug delivery, counterion concentration is dependent on the physiological environment and beyond user control.

Here we show that coating DNA-assembled nanoparticles with cationic polymers can enhance their structure and properties beyond the native environment from which they were synthesized. Specifically, we show that substituting sodium or magnesium cations with polyamines of specific lengths rigidified DNA-assembled nanoparticles and reduced interparticle spacing. In the case of metal nanoparticles, this reduction in interparticle spacing also enhanced plasmon coupling. Similar to how histones package DNA in nucleosomes, these novel properties result from the ability of polyvalent amines to condense DNA. We further show that polyamine coated DNA assemblies provide a scaffold to create new materials based on the layer-by-layer assembly method. We

propose that in general, polyvalent counterions can be designed to engineer the structure and properties of DNA-assembled nanostructures for downstream applications.

RESULTS AND DISCUSSION

DNA Assembly of Metal Nanoparticle Superstructures. This study focused on a specific nanoparticle assembly geometry commonly referred to as "core–satellite" (Figure 1A). This geometry features a number of tunable parameters
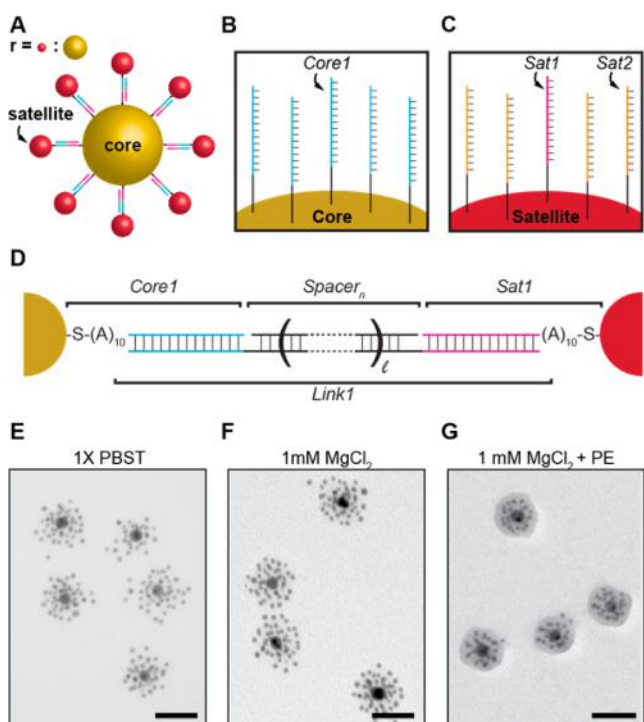
Figure 1. DNA assembly of gold nanoparticles into "core-satellite" superstructures. (A) Schematic of the superstructure showing satellite nanoparticles in red and core nanoparticle in yellow. Parameters varied in this study were diameters of the core and satellite (d_{core} and d_{sat}) as well as their stoichiometry (r). (B) Core nanoparticles were grafted with a single 25 nt sequence (*Core1*) while (C) satellites were grafted with two 25 nt sequences (*Sat1* and *Sat2*). (D) *Link1* was used to connect *Core1* to *Sat1* separated by 60 nt. This single-stranded region was used to attach a number of spacer strands (denoted *Spacer$_n$*) conjugated with fluorophores. (E) Representative TEMs of core–satellite superstructures after resuspension in 1× PBST, (F) 1 mM MgCl$_2$, and after (G) polyelectrolyte coating (PE) in 1 mM MgCl$_2$. Scale bars = 50 nm.

which have been theoretically studied in the context of plasmon engineering[12] as well as experimentally implemented using various types of linkers,[12−16] making it a well-defined model system. As building blocks for assembling core–satellite superstructures, we synthesized gold nanorods and spherical gold nanoparticles of 5, 15, 30, and 60 nm in diameter and grafted them with single-stranded, thiolated oligonucleotides according to published procedures.[17−19] Nanoparticles designated as the "core" were grafted with a 25 nt oligonucleotide sequence (*Core1*) for linking to "satellite" nanoparticles (Figure 1B). Nanoparticles designated as "satellites" were grafted with two different sequences of oligonucleotides of 25 nt each (*Sat1* and *Sat2*, Figure 1C). In this mixed monolayer, *Sat1* was used for the purpose of assembly while *Sat2* is a noncomplementary sequence used to fill vacant binding sites on the satellite

nanoparticle surface. We kept the *Sat1*-to-*Sat2* grafting stoichiometry low (1:4) to minimize cross-linking superstructures into macroscopic aggregates. This mixed monolayer strategy was useful for maximizing the surface charge density of satellite nanoparticles, which improved their colloidal stability and subsequent interactions with cationic polyelectrolytes. Oligonucleotide grafting onto nanoparticles was performed according to the pH-assisted method of Liu et al.,[19] which we found to be superior to the conventional salt-aging method in that similar grafting densities were obtained within 30 min of incubation instead of hours to days (e.g., 85 ± 6.0 strands per 15 nm nanoparticle and 66 ± 2.4 strands per nanorod, see Figure S1). To initiate assembly, "core" nanoparticles were first incubated with an excess of 90 nt linker strand (*Link1*, Figure 1D), isolated by centrifugation, and then incubated with 100× molar excess of "satellite" nanoparticles. *Link1* contains a single-stranded region that binds one to several spacer strands (denoted *Spacer$_n$* in Figure 1D), which we used to incorporate other molecules within the core–satellite. Assembled superstructures were washed by centrifugation and stored in phosphate buffered saline containing 0.01% w/v Tween20 (PBST). Transmission electron microscopy (TEM) showed that superstructures were uniform in size and well dispersed (Figure 1E and Figure S2).

Polyamines Compact DNA–Metal Superstructures. To integrate core–satellite superstructures with polyamines, we first buffer exchanged them into 1 mM MgCl$_2$. This step was important, since initial attempts at exposing superstructures to various types of cationic polyelectrolytes in PBST resulted in colloidal aggregation and precipitation (Figure S3A,B). In contrast, the presence of low millimolar concentrations of magnesium maintained both the stability of the DNA duplex and the colloidal stability of DNA-assembled metal nanoparticle superstructures as determined by fluorescence and spectrophotometric assays (Figure S3C,D), as well as TEM (Figure 1F). Buffer exchanged superstructures were added dropwise into a solution of cationic polyelectrolytes such as poly(allylamine) and vigorously stirred for 1 to 2 h. Superstructures were purified from excess polyelectrolytes by centrifugation and re-examined under TEM (Figure 1G). Comparing superstructure morphology before and after polyelectrolyte coating, we noted two interesting observations. First, polyelectrolyte coating preserved the discrete, colloidal nature of the superstructures and the core–satellite morphology. Second, coating reduced the spacing between nanoparticles and the overall size of the superstructures. These observations were confirmed by dynamic light scattering measurements, which showed unimodal size distribution and a decrease in the hydrodynamic size of the superstructures following polyelectrolyte coating (Figure 2A). For core–satellites assembled using 15 and 5 nm gold nanoparticles, the hydrodynamic diameter decreased from 87 to 62 nm after polyelectrolyte coating. On the basis of a quasi-spherical geometry, this size reduction corresponded to a remarkable 2.8-fold volumetric compression, consistent with the known ability of polyvalent cations to condense DNA.[20−23]

To confirm the condensation of DNA in solution, we attached Cy5-labeled spacer strands (*Spacer$_2$*-Cy5) to *Core1*/*Link1*-functionalized 15 nm gold nanoparticles (Figure 2B). These particles were then incubated with poly(allylamine) as described in the previous section. Fluorescence measurements showed that polyelectrolyte coating decreased Cy5 fluorescence intensity by 87% compared to noncoated nanoparticles (Figure 2B). Since metals quench fluorophores in a distance-dependent
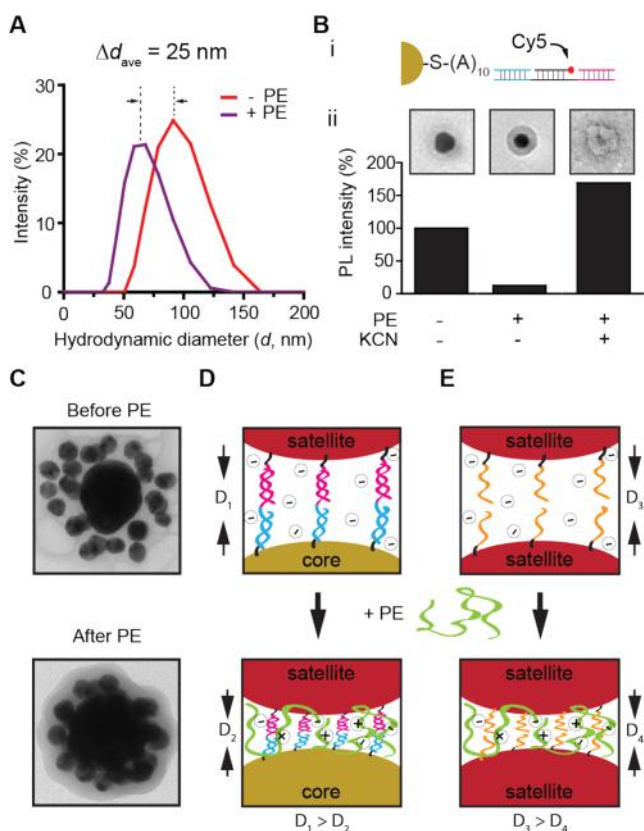
Figure 2. Compaction of polyelectrolyte coated core–satellites. (A) Hydrodynamic diameter of core–satellites (d_{core} = 15 nm, d_{sat} = 5 nm, r = 30:1) before and after polyelectrolyte coating. (B) Fluorescence of Cy5-labeled oligonucleotides on the nanoparticle surface before and after polyelectrolyte and potassium cyanide treatment. (i) Position of the Cy5 label. (ii) Cy5 fluorescence and corresponding TEM of materials following treatment. (C) TEM of core–satellite (d_{core} = 60 nm, d_{sat} = 30 nm, r = 30:1) before and after polyelectrolyte coating. (D,E) Proposed model of two mechanisms by which polyelectrolytes interact with and compact the structure. PE: polyelectrolyte coat; KCN: potassium cyanide.

manner,[24−26] this result suggests that Cy5-labeled oligonucleotides moved closer to the nanoparticle surface following polyelectrolyte coating. Removal of the gold core by potassium cyanide dissolution restored the fluorescence by 150%, confirming that fluorophore interactions with the metal (e.g., not the amines)[27] accounted for the majority of quenching. We further confirmed structural compaction as a result of DNA condensation using TEM. Figure 2C shows representative images of superstructures consisting of 60 nm core and 15 nm satellite nanoparticles, before and after exposure to poly-(allylamine). The polymer layer appeared as a shell around the superstructure, and reduced spacing both between core and satellites as well as between neighboring satellite nanoparticles. On the basis of these observations, we propose that polyamines can (1) compact DNA nanostructures through DNA condensation (Figure 2D), and (2) cross-link neighboring nanoparticles through polyvalent interactions with multiple DNA strands (Figure 2E). The latter further contributes to structural compaction, and may also improve the mechanical stability of the nanostructure.

Polyelectrolytes Enhance Plasmon Coupling of DNA–Metal Superstructures. We hypothesized that the ability of polyamines to compact metal superstructures may enhance plasmon-coupling efficiency, which is known to vary as a function of interparticle distance. To test this, we fabricated two sets of assembly designs each consisting of 60 nm gold nanoparticle cores linked with either 15 or 30 nm satellites (Figure 3A,B). The relatively large core size was chosen based on the motivation that its large extinction cross-section would allow us to directly visualize plasmon coupling enhancement, whereas the two different satellite sizes would allow us to compare the effects of assembly design on plasmon coupling efficiency following interactions with polyelectrolytes. Indeed, upon exposure to polyelectrolytes, we observed immediate change in the color of the colloidal solutions changed from red to different hues of blue and purple (Supplementary Video 1). The final colors varied as a function of both the size of the core and satellite nanoparticles and their assembly stoichiometry (Figure 3C,D). These differences were quantified using UV−vis spectrophotometry as shown in Figures 3E,F. Before polyelectrolyte addition, the absorption spectra of both sets of designs were dominated by a single peak at 550 nm, associated with the surface plasmon resonance mode of single spherical 60 nm gold nanoparticles (Figure 3E,F, "before PE"). For both satellite designs, the addition of polyelectrolytes resulted in significant redshift in the surface plasmon resonance absorption, and in broadening of the absorption line width. These patterns are indicative of increased dampening of plasmon charge oscillations and the generation of higher order plasmon modes, reflecting enhanced plasmon coupling between assembled nanoparticles. Polyelectrolytes also augmented the impact of design on the optical response of the nanostructures. Figure 3E shows that increasing satellite-to-core stoichiometry from 3 to 30 in the absence of polyelectrolytes corresponded to a 5 nm redshift in UV−vis absorption. In contrast, the same design red-shifted by 70 nm following polyelectrolyte addition (Figure 3E, "after PE"). Similar trends could be observed for the 30 nm satellite design by comparing the "Before PE" panel to the "After PE" panel in Figure 3F. Overall, the largest enhancement was observed in assemblies consisting of 60 nm core and 30 nm satellite nanoparticles with the highest satellite-to-core stoichiometry. Here, the addition of polyelectrolytes generated a new absorption peak at 670 nm, corresponding to a 120 nm redshift from the original peak of 550 nm (Figure 3F, v).

Interestingly, we reproduced these same trends using poly(L-lysine) as another cationic polyelectrolyte, suggesting that enhancement is not restricted to one type of polyamine. We further examined the effects of polyamine length on plasmon coupling by coating DNA−metal superstructures with poly(L-lysine) consisting of 5, 10, 30, 100, or 250 repeat units (Figure S4). UV−vis spectrophotometry showed sharp transition in enhancement at a chain length of 10 monomers. Chain lengths longer than 10 monomers led to diminishing increases in plasmon enhancement, whereas chain length smaller than 10 did not result in enhancement. These observations are consistent with the hypothesis that the degree of DNA condensation controls structural compaction and plasmon enhancement, and that these properties are tunable as a function of polyamine length (e.g., valency).

Layer-by-Layer Encapsulation of DNA−Metal Superstructures. Polyamine coated DNA−metal superstructures exhibited uniform morphology and excellent colloidal stability. This prompted us to hypothesize that in general, DNA nanostructures can be used as supramolecular scaffolds to template polyelectrolyte deposition using the layer-by-layer
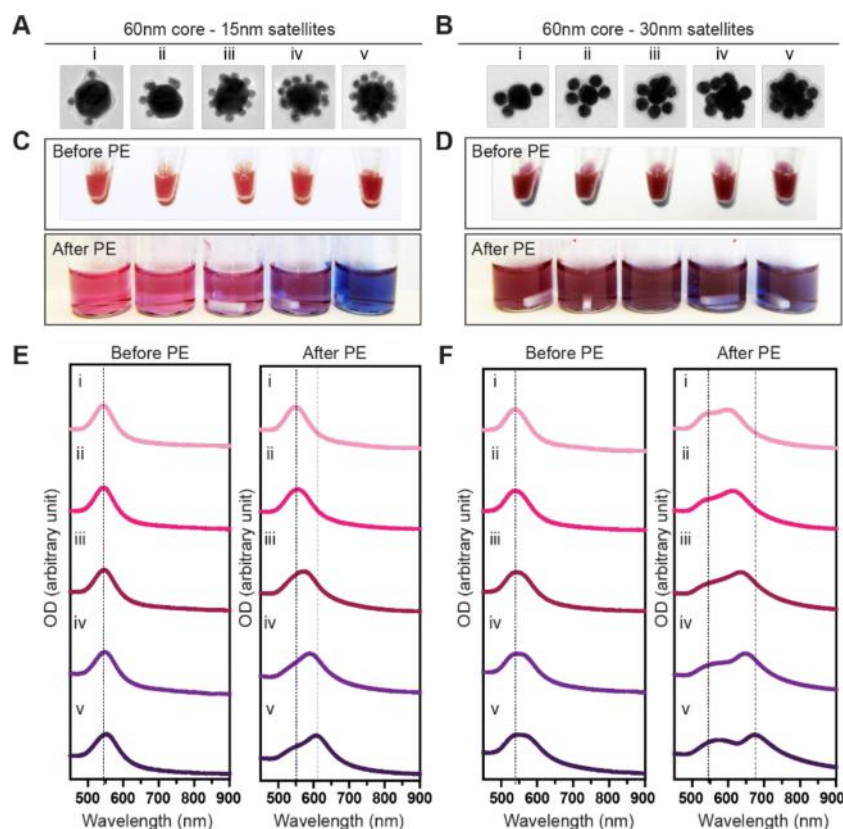
Figure 3. Polyelectrolyte coating enhances plasmon coupling of core−satellites. (A,B) TEM of two sizes of core−satellite structures, with satellite-to-core stoichiometry increasing from 3:1 to 30:1 (i−v). (C,D) Corresponding colors of the core−satellite solutions before and after polyelectrolyte coating (PE). (E,F) Corresponding UV−vis absorbance spectra of the core−satellite solutions shown in C and D. OD: optical density.
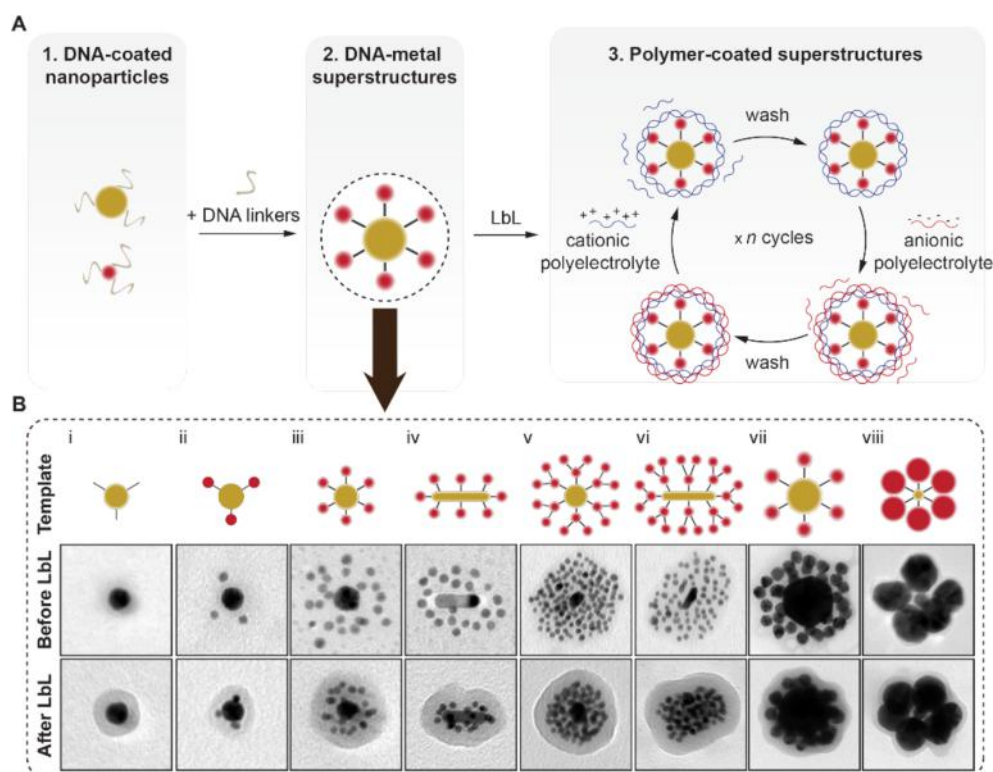
Figure 4. Encapsulation of metal superstructures using the layer-by-layer technique. (A) Schematic of the layer-by-layer fabrication procedure. (B) Morphological transition of eight different metal superstructures before and after coating with four cycles of poly(allylamine) and poly(styrenesulfonate). LbL: layer-by-layer.

assembly method[28,29] (Figure 4A). If so, polyelectrolyte engineering and deposition would be a versatile synthetic strategy to improve the structural integrity and functionality of DNA-based nanomaterials. To test this, we performed layer-by-layer assembly on a panel of eight DNA-assembled metal nanostructures with varying size, shape, and assembly architectures, using poly(allylamine) and poly-(styrenesulfonate) as the model polyelectrolyte pair (Figure 4B). Under TEM, we observed successful growth of polyelectrolyte multilayers around all the structures tested, evidenced by the appearance of a uniform polymer shell (Figure 4B, "after LbL"). Zeta potential measurements further demonstrated robust surface charge reversal following each round of deposition (Figure S5). Similar to our previous results, polyelectrolyte deposition induced structural compaction in all the DNA−metal superstructures while preserving the overall geometry of the assembly (Figure 4B).

We further characterized three selected layer-by-layer coated nanostructures by scanning electron microscopy (Figure 5A, i−
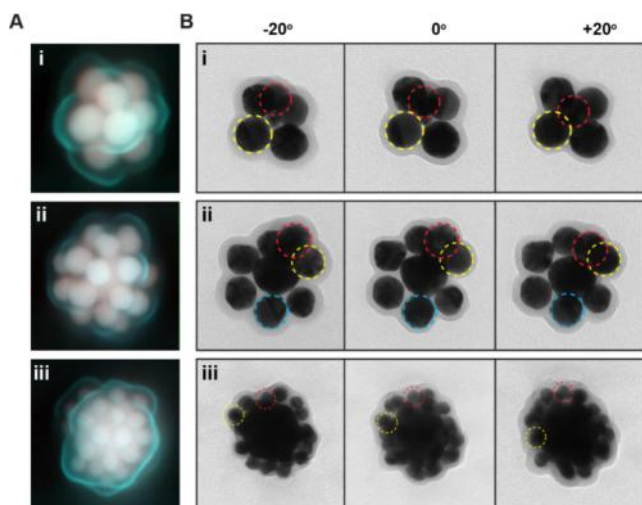

Figure 5. Structural examination of layer-by-layer coated DNA−metal superstructures. (A) SEM of three different superstructures following LbL assembly: (i) d_{core} = 15 nm, d_{sat} = 30 nm, r = 6:1; (ii) d_{core} = 60 nm, d_{sat} = 30 nm, r = 20:1; (iii) d_{core} = 60 nm, d_{sat} = 15 nm, r = 30:1. Polyelectrolyte coatings are false-colored in cyan and nanoparticles in white. (B) Tilt-angle TEM showing the 3D architecture of the superstructures following polyelectrolyte coating. (i−iii) correspond to the three designs shown in (A).

iii). By separately detecting both secondary and backscattered electrons, the polyelectrolyte coating (cyan) could be clearly distinguished from the inorganic nanoparticles (white). Although each superstructure displayed a quasi-spherical morphology overall, the polyelectrolyte can be seen to wrap around the contour of individual nanoparticles, suggesting they cross-link nanoparticles through electrostatic interactions with the attached DNA. To better understand the morphology of layer-by-layer coated nanostructures, we characterized them by tilted-angle TEM, in which the plane of observation was rotated about the z-axis by a total of 40° (Figure 5B, i−iii). Comparing change in nanoparticle orientation as a function of tilt angle (e.g., dotted circles in Figure 5B) with nonpolyelectrolyte coated controls, we believe that polyelectrolyte multilayers also enhanced the structural rigidity of DNA−metal superstructures (see discussion in Figure S6).

Polyelectrolyte Composition Adds Functionality to DNA−Metal Superstructures.

Plasmonic nanostructures have applications as biological imaging agents and sensors, but nanostructures assembled from DNA lack long-term stability and are destroyed quickly by endogenous nucleases. In contrast, we found that layer-by-layer coated DNA−metal nanoparticle superstructures remained stable for at least one month when stored in 1 mM $MgCl_2$ or deionized water at 4 °C, as determined by TEM (Figure S7). Coating also protected superstructures against nuclease degradation as demonstrated by a DNase I assay (Figure S8). Enzymatic degradation was tunable as a function of polyelectrolyte composition. For example, trypsin is a serine protease that breaks down proteins by catalyzing the hydrolysis of peptide bonds. For super-structures coated with the polypeptides poly(L-lysine) and poly(L-glutamic acid), incubation with trypsin resulted in blueshift of their plasmon absorption pattern back to the state before layer-by-layer assembly. This was accompanied by disappearance of the polyelectrolyte layer around the super-structures when examined under TEM (Figure 6B, from state i
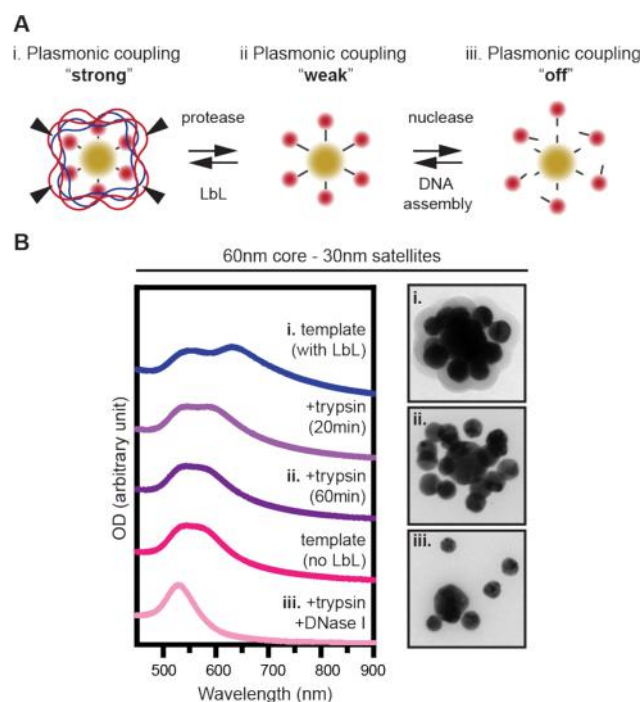
Figure 6. Tuning plasmonic response of LbL-encapsulated metal superstructures to environmental stimuli. (A) Three distinct plasmon-coupling states in response to protease and nuclease degradation. (B) UV−vis absorbance spectra and corresponding TEM of core−satellites (d_{core} = 60 nm, d_{sat} = 30 nm, r = 20:1). Spectrum of the core−satellite without coating (no LbL) is included for reference. LbL: layer-by-layer.

to state ii). Further blueshift in the absorption spectra to that of the nonassembled state, was observed with the addition of both DNase I and trypsin (Figure 6B, from state ii to iii), suggesting that enzyme combinations can toggle different optical responses. On the other hand, for superstructures coated with poly(allylamine) and poly(styrene-sulfonate), which do not contain peptide bonds in their backbone, the optical response of the superstructures was unchanged after incubation with either DNase I or trypsin, or a combination of these enzymes (Figure S9). Together, these results highlight the use of

polyelectrolyte composition to customize the structure and properties of DNA-assembled nanoparticles for downstream applications.

CONCLUSION

In this study, we showed that polyamines enhance the structural rigidity and plasmon coupling of DNA–metal superstructures through nanoparticle cross-linking and DNA condensation. Unlike sodium and magnesium ions, interaction between polyamines and DNA is polyvalent and long-lived, where the degree of avidity can be tuned as a function of polymer chain length. In this regard, the use of polyamine-based counterions for engineering the properties of DNA-assemblies deserves further development. For example, future work can elucidate whether regimes of structural rigidity and compaction can be separated with the appropriate structure of polyamine, as the two effects can be desirable for different applications. The incorporation of other types of environmentally responsive polyamines and polyelectrolytes to DNA-based nanomaterials can also be useful. For example, thiol- or acid-responsive polyelectrolytes can be used to report on the intracellular location of plasmonic probes or the release of payloads through a change in the optical response. To engineer more complex optical properties, methods such as DNA origami could be employed to further control the geometry and composition of nanoparticle assembly.[30] Integration of such nanostructures with polyamines merits further exploration. In conclusion, the appropriate design of counterion chemistry and fine-tuning of DNA-counterion interactions have important implications for practical applications of DNA nanostructures.

EXPERIMENTAL PROCEDURES

Materials. Sources of all the reagents used in this study are listed in Supporting Table S1.

Gold Nanoparticle Synthesis. Gold nanoparticles of 15 nm in diameter were synthesized by adding $HAuCl_4$ (1 mL, 1% w/v) to Nanopure water (98 mL) in a 250 mL Erlenmeyer flask. The solution was brought to a boil on a hot place set to 300 °C, and trisodium citrate (1 mL, 3% w/v) was injected swiftly into the flask while the reaction mixture is under vigorous stirring. The reaction was allowed to take place for 7 min and then quenched on ice. Nanoparticles were washed by centrifugation at 4 °C and 13 000g for 30 min in Tween 20 (0.01% w/v).

Gold nanoparticles of 5 nm in diameter were synthesized by adding $HAuCl_4$ (1 mL, 1% w/v) to Nanopure water (79 mL) in a 250 mL Erlenmeyer flask heated on a hot plate at 60 °C. A reducing solution was prepared by mixing water (16 mL), tannic acid (1 mL, 1% w/v), trisodium citrate (4 mL) and potassium bicarbonate (1 mL, 3.46 mg/mL). The reducing solution was heated to 60 °C and injected swiftly into the reaction mixture under vigorous stirring. The reaction was allowed to take place at 60 °C for 30 min and at 90 °C for 10 min, and then quenched on ice. Nanoparticles were stabilized by overnight incubation with bis(p-sulfonatophenyl)-phenylphosphine dihydrate dipotassium salt (0.8 mg/mL) while stirring, and washed by ultracentrifugation two times at 4 °C and 250 000g for 30 min in Tween 20 (0.01% w/v).

Gold nanoparticles of 30 nm and 60 nm in diameter were synthesized according to previously published procedures.[18] Briefly, 15 nm nanoparticle "seeds" were added to Nanopure H_2O in a 250 mL Erlenmeyer flask, followed by addition of $HAuCl_4$ (1 wt %) and trisodium citrate (4.1 mg/mL) as stabilizers. A solution of hydroquinone (3.3 mg/mL) was then swiftly injected into the solution under vigorous stirring to reduce gold ions onto seed surface. The reaction was allowed to take place overnight at room temperature for completion. Synthesized particles were washed three times with washing buffer containing sodium citrate (0.1 mg/mL) and Tween20

(0.05% w/v). The size of the particle was controlled by changing the stoichiometry of seeds to gold solution as detailed in Supporting Table S2. Nanoparticles were washed three times by centrifugation at 4 °C, using 4000g for 30 nm and 1000g for 60 nm nanoparticles for 30 min in Tween 20 (0.01% w/v).

Gold nanorods with aspect ratio of 4.1 ± 0.2 were synthesized from a seed solution created by adding 1.2 mL of sodium borohydride (0.01 M) to a 20 mL scintillation vial containing 500 μL of $HAuCl_4$ (0.01 M) and 19.5 mL of cetyltrimethylammonium bromide (CTAB, 0.1 M) under vigorous stirring. In a clean bottle, 49.5 mL of 0.01 M $HAuCl_4$ was added to 950 mL of CTAB (0.1 M). To this solution, 5 mL of $AgNO_3$ (0.01 M) and 7 mL of ascorbic acid (0.1 M) were added respectively under stirring. Finally, 20 mL of the above prepared seed solution was added and the entire solution was left overnight under stirring. The obtained gold nanorod solution was then purified by centrifugation twice at 17 000g for 20 min and redispersed in water to remove excess CTAB.

Synthesized nanoparticles were characterized using TEM, UV–vis spectrophotometry, and dynamic light scattering.

Oligonucleotide Grafting. Spherical gold nanoparticles were functionalized with thiolated DNA using a previously published method.[19] Briefly, 15 nm gold nanoparticles (25 nM) were mixed with thiolated *Core1* (3.75 μM) in the presence of Tween20 (0.01% w/v) and trisodium citrate (30 mM, pH 3.0). The mixture was incubated for 30 min and DNA functionalized gold nanoparticles were purified by centrifugation at 16 000g for 30 min at 4 °C using 1× phosphate buffered saline containing Tween20 (0.01% w/v) as the solvent. Five nm gold nanoparticles (100 nM) were coated with a mixture of thiolated *Sat1* and *Sat2* (ratio = 3:7, 2 μM overall) using the same buffer as for the 15 nm gold nanoparticles. Oligonucleotide coated 5 nm nanoparticles were washed and isolated by ultracentrifugation two times at 250 000g for 30 min at 4 °C in 1× PBST. Samples were stored at 4 °C. The amount of oligonucleotides used for grafting larger spherical nanoparticles was scaled to maintain constant oligonucleotide concentration per nanoparticle surface area.

Gold nanorods were washed twice in water by centrifugation at 13 000g for 30 min at room temperature. Nanorods were next added to solution containing sodium dodecyl sulfate (0.2% w/v) and thiolated oligonucleotides in 500× molar excess. A solution of 2× tris-borate-EDTA (TBE) containing sodium chloride (1 M) at pH 3.0 was added in equal volume to the nanorod solution to facilitate the grafting of oligonucleotides onto the nanorod. The solution was incubated overnight in a 37 °C bath, and then washed twice at 15 000g for 35 min at 30 °C using 1× PBS with 0.01% w/v Tween 20. The concentration of the nanorods was measured by UV–vis absorbance at 740 nm. Samples were stored at 4 °C prior to use.

Nanoparticle Grafting Density. Density of oligonucleotides on nanoparticles was determined as previously described.[31] Briefly, nanoparticle concentration was determined by UV–vis spectrophotometry using published molar extinction coefficients of the nanoparticles.[32] Nanoparticles were then incubated with dithiothreitol (10 mM) at 60 °C for 30 min to liberate the grafted oligonucleotides and pelleted by centrifugation at 16 000g for 30 min to remove the aggregates. Oligonucleotide concentration in the supernatant was determined using the Oligreen reagent and compared with standards that have undergone identical treatment. The average oligonucleotides grafting density per nanoparticle was determined by dividing the oligonucleotide concentration to the nanoparticle concentration.

Nanoparticle Assembly. DNA assembly was performed according to previously published methods with some modifications.[31] Briefly, *Core1* oligonucleotide functionalized 15 nm gold nanoparticles (10 nM) were mixed with *Link1* oligonucleotides (1 μM) in hybridization buffer consisting of 3× phosphate buffered saline containing magnesium chloride (5 mM) and Tween20 (0.01% w/v). The mixture was incubated in a 60 °C water bath for 10 min and then incubated in a 37 °C incubator for 1 h. The mixture was then taken out and cooled to room temperature for 20 min, and washed by centrifugation 2 times at 4 °C and 16 000g for 30 min using 1× PBST to remove excess *Link1* oligonucleotides.

Purified *Link1*-functionalized nanoparticles (10 nM) were mixed with spacer strands *Spacer1* and *Spacer2* or their fluorophore-labeled versions at 100:1 molar excess relative to nanoparticles in hybridization buffer. Particles were incubated in a 37 °C incubator for 1 h. Satellite nanoparticles suspended in hybridization buffer were then added to this mixture at 100:1 molar excess relative to the core nanoparticles, and incubated at 37 °C for 1 h. Assembled superstructures were cooled at room temperature for 30 min, and then washed 4 times by centrifugation at 11 000*g* and 4 °C for 30 min using 1× PBST. Finally, superstructures (2 nM) were incubated with *Link2* (0.4 μM) in hybridization buffer at 37 °C for 1 h, followed by washing three times in 1× PBST at 4 °C and 16 000*g* for 30 min. *Link2* was used to improve colloidal stability of the assembly in solution. After the last wash, superstructures were stored at 4 °C prior to use. The assembly of larger sizes of spherical nanoparticles followed the same procedures, with the single modification that nanoparticle concentration was reduced to maintain constant total surface area. For example, we used approximately 16× lower concentration of 60 nm core gold nanoparticles (0.6 nM) in the assembly reaction than 15 nm core gold nanoparticles (10 nM).

Assay of Colloidal Stability for Polyelectrolyte Coating. DNA-functionalized gold nanoparticles were suspended in water and mixed with aqueous solutions of cationic polyelectrolytes (8 mg/mL) titrated with different concentrations of either sodium chloride or magnesium chloride. Three compositions of polyelectrolytes, namely poly(L-lysine), poly(L-arginine), and poly(allylamine), were tested in parallel. The mixtures were incubated at room temperature for 1 h. An aliquot from each mixture was centrifuged at 13 000*g* for 30 min to pellet the nanoparticles and resuspended in the same solvent. Colloidal stability was evaluated by measuring the UV−vis absorbance profile of the nanoparticle solutions before and after centrifugation. The extent of aggregation was determined by taking the ratio of absorbance at 520 to 700 nm. Results were compared to controls of nanoparticles in water.

Assay of dsDNA Stability on Nanoparticles. FAM-labeled *Link1* was attached to *Core1*-functionalized gold nanoparticles as described in the previous section. 8-methoxypsoralen (20 mM in DMSO) was added to nanoparticles to a final concentration of 500 μM. Nanoparticles were exposed to UV on ice using a hand-held UV-lamp for 30 to 120 min to induce UV cross-linking of oligonucleotides. Following cross-linking, nanoparticles were buffer exchanged into either water, 1 mM magnesium chloride, or sodium chloride by centrifugation two times. Oligonucleotides that remained on the nanoparticle were removed by addition of freshly prepared dithiothreitol (100 mM) followed by incubating the mixture at 60 °C for 30 min. Nanoparticle aggregates were pelleted. FAM-labeled oligonucleotide standards were prepared using identical procedures and used for quantification.

Polyelectrolyte Coating. Before polyelectrolyte coating, DNA-assembled metal nanoparticle superstructures were buffer exchanged into 1 mM magnesium chloride by centrifugation. The buffered exchanged nanoparticle solution (0.1 mL, 10 nM) was then dropwise added to 1 mM magnesium chloride solution containing polyelectrolytes (1 mL, 8 mg/mL) under vigorous stirring. For a single layer coating, either poly(L-lysine) or poly(allylamine) was used as the cationic polyelectrolyte to complex with the anionic oligonucleotides displayed on the surface of the nanoparticles. The solution was stirred for 1 h before washing twice by centrifugation at 8000*g* and 4 °C for 45 min using 1 mM magnesium chloride as solvent. For layer-by-layer assembly, the aforementioned polyelectrolyte coating procedure was repeated using polyelectrolytes of alternating charges.

Experiments with different molecular weights of poly(L-lysine) were performed similarly with slight modifications. Poly(L-lysine) with chain length (*n*) of 5, 10, 30, 100, or 250 were dissolved in water, pH adjusted to 7, and 5× serially diluted from 10 mg/mL to 0.001 mg/mL. Nanoparticles were added to these working solutions the same way as described above and subsequently purified by centrifugation.

Scanning Electron Microscopy. Scanning electron micrographs of nanoparticle assemblies shown in Figure 5A were obtained using a Hitachi S-5200 high resolution SEM equipped with two detectors to detect both secondary (SE) and backscattered electrons (BSE). SE mode was used to image the organic polyelectrolyte coating, while the gold nanoparticles were imaged under BSE mode. Images were false colored separately in ImageJ (nanoparticles in white, polyelectrolyte coating in cyan) and combined to visualize the coating.

Trypsin and DNase I Treatment. Superstructures (10 μL, 0.1 nM) were incubated either with trypsin (10 μL, 0.1% v/v), DNase I (10 μL, 1 U/μL) or both in 1× PBST at 37 °C for 60 min. The stability of the polyelectrolyte shell and the integrity of the DNA assembly were evaluated by monitored by measuring the UV−vis absorbance of the material. Samples treated with trypsin, DNase I or both were directly drop casted onto copper grids for TEM.

■ ASSOCIATED CONTENT

Ⓢ Supporting Information
The Supporting Information is available free of charge on the ACS Publications website at DOI: 10.1021/jacs.6b00751.

> Supporting Figures S1−9, synthesis recipes for 30 and 60 nm gold nanoparticles, and list of materials and oligonucleotides used in this study. (PDF)
> Supporting movie. (MPG)

■ AUTHOR INFORMATION

Corresponding Author
*warren.chan@utoronto.ca

Present Address
#Wyss Institute for Biologically Inspired Engineering, Harvard University, CLSB 5th floor, Three Blackfan Circle, Boston, Massachusetts 02115, United States.

Author Contributions
∇L.Y.T.C and F.S. contributed equally.

Notes
The authors declare no competing financial interest.

■ ACKNOWLEDGMENTS

■ REFERENCES

(1) Jones, M. R.; Seeman, N. C.; Mirkin, C. A. *Science* **2015**, *347* (6224), 1260901.
(2) Tan, S. J.; Campolongo, M. J.; Luo, D.; Cheng, W. *Nat. Nanotechnol.* **2011**, *6* (5), 268.
(3) Barrow, S. J.; Funston, A. M.; Wei, X.; Mulvaney, P. *Nano Today* **2013**, *8* (2), 138.
(4) Castro, C. E.; Kilchherr, F.; Kim, D.-N.; Shiao, E. L.; Wauer, T.; Wortmann, P.; Bathe, M.; Dietz, H. *Nat. Methods* **2011**, *8* (3), 221.
(5) Randeria, P. S.; Jones, M. R.; Kohlstedt, K. L.; Banga, R. J.; Olvera de la Cruz, M.; Schatz, G. C.; Mirkin, C. A. *J. Am. Chem. Soc.* **2015**, *137* (10), 3486.
(6) Lermusiaux, L.; Maillard, V.; Bidault, S. *ACS Nano* **2015**, *9* (1), 978.
(7) Jin, R.; Wu, G.; Li, Z.; Mirkin, C. A.; Schatz, G. C. *J. Am. Chem. Soc.* **2003**, *125* (6), 1643.
(8) Seferos, D. S.; Prigodich, A. E.; Giljohann, D. A.; Patel, P. C.; Mirkin, C. A. *Nano Lett.* **2009**, *9* (1), 308.
(9) Park, S.-J.; Lazarides, A. A.; Storhoff, J. J.; Pesce, L.; Mirkin, C. A. *J. Phys. Chem. B* **2004**, *108* (33), 12375.

(10) Busson, M. P.; Rolly, B.; Stout, B.; Bonod, N.; Larquet, E.; Polman, A.; Bidault, S. *Nano Lett.* **2011**, *11* (11), 5060.

(11) Barrow, S. J.; Funston, A. M.; Gómez, D. E.; Davis, T. J.; Mulvaney, P. *Nano Lett.* **2011**, *11* (10), 4180.

(12) Ross, B. M.; Waldeisen, J. R.; Wang, T.; Lee, L. P. *Appl. Phys. Lett.* **2009**, *95* (19), 193112.

(13) Dey, P.; Zhu, S.; Thurecht, K. J.; Fredericks, P. M.; Blakey, I. *J. Mater. Chem. B* **2014**, *2* (19), 2827.

(14) Gandra, N.; Abbas, A.; Tian, L.; Singamaneni, S. *Nano Lett.* **2012**, *12* (5), 2645.

(15) Gandra, N.; Singamaneni, S. *Chem. Commun.* **2012**, *48* (94), 11540.

(16) Sebba, D. S.; Lazarides, A. A. *J. Phys. Chem. C* **2008**, *112* (47), 18331.

(17) Perrault, S. D.; Chan, W. C. W. *J. Am. Chem. Soc.* **2009**, *131* (47), 17042.

(18) Chou, L. Y. T.; Chan, W. C. W. *Adv. Healthcare Mater.* **2012**, *1* (6), 714.

(19) Zhang, X.; Servos, M. R.; Liu, J. *J. Am. Chem. Soc.* **2012**, *134* (17), 7266.

(20) Bloomfield, V. A. *Curr. Opin. Struct. Biol.* **1996**, *6* (3), 334.

(21) Koltover, I.; Wagner, K.; Safinya, C. R. *Proc. Natl. Acad. Sci. U. S. A.* **2000**, *97* (26), 14046.

(22) Widom, J.; Baldwin, R. L. *J. Mol. Biol.* **1980**, *144* (4), 431.

(23) Vijayanathan, V.; Thomas, T.; Shirahata, A.; Thomas, T. J. *Biochemistry* **2001**, *40* (45), 13644.

(24) Anger, P.; Bharadwaj, P.; Novotny, L. *Phys. Rev. Lett.* **2006**, *96* (11), 113002.

(25) Schneider, G.; Decher, G.; Nerambourg, N.; Praho, R.; Werts, M. H. V.; Blanchard-Desce, M. *Nano Lett.* **2006**, *6* (3), 530.

(26) Dulkeith, E.; Morteani, A. C.; Niedereichholz, T.; Klar, T. A.; Feldmann, J.; Levi, S. A.; van Veggel, F. C. J. M.; Reinhoudt, D. N.; Möller, M.; Gittins, D. I. *Phys. Rev. Lett.* **2002**, *89* (20), 203002.

(27) Van, S.-P.; Hammond, G. S. *J. Am. Chem. Soc.* **1978**, *100* (12), 3895.

(28) Li, Y.; Wang, X.; Sun, J. *Chem. Soc. Rev.* **2012**, *41* (18), 5998.

(29) Tong, W.; Song, X.; Gao, C. *Chem. Soc. Rev.* **2012**, *41* (18), 6103.

(30) Tian, Y.; Wang, T.; Liu, W.; Xin, H. L.; Li, H.; Ke, Y.; Shih, W. M.; Gang, O. *Nat. Nanotechnol.* **2015**, *10* (7), 637.

(31) Chou, L. Y. T.; Zagorovsky, K.; Chan, W. C. W. *Nat. Nanotechnol.* **2014**, *9* (2), 148.

(32) Jain, P. K.; Lee, K. S.; El-Sayed, I. H.; El-Sayed, M. A. *J. Phys. Chem. B* **2006**, *110* (14), 7238.